


Article

Influence of Saline Buffers over the Stability of High-Annealed Gold Nanoparticles Formed on Coverslips for Biological and Chemosensing Applications

Lan Zhou and Rodica Elena Ionescu * 

Laboratory Light, Nanomaterials and Nanotechnologies - L2n, CNRS ERL 7004, University of Technology of Troyes, 12 rue Marie Curie, 10004 Troyes, France; lan.zhou@utt.fr

* Correspondence: elena_rodica.ionescu@utt.fr; Tel.: +33-3-2575-9728; Fax: +33-3-2571-8456

Received: 29 May 2020; Accepted: 30 June 2020; Published: 3 July 2020



Abstract: Herein, coverslips were used as solid supports for the synthesis of gold nanoparticles (AuNPs) in three steps: (i) detergent cleaning, (ii) evaporation of 4 nm gold film and (iii) exposure at high annealing temperature (550 °C) for 3 h. Such active gold nanostructured supports were investigated for their stability performances in aqueous saline buffers for new assessments of chemical sensing. Two model buffers, namely saline-sodium phosphate-EDTA buffer (SSPE) and phosphate buffer saline (PBS), that are often used in the construction of (bio)sensors, are selected for the optical and microscopic investigations of their influence over the stability of annealed AuNPs on coverslips when using a dropping procedure under dry and wet media working conditions. A study over five weeks monitoring the evolution of the localized surface plasmon resonance (LSPR) chemosensing of 1,2-bis-(4-pyridyl)-ethene (BPE) is discussed. It is concluded that the optimal sensing configuration is based on annealed AuNPs exposed to saline buffers under wet media conditions (overnight at 4 °C) and functionalized with BPE concentrations (10^{-3} – 10^{-11} M) with the highest LSPR spectra after two weeks.

Keywords: stability of annealed gold nanoparticles; saline buffers; BPE sensing

1. Introduction

Metallic nanoparticles are attractive active supports for various optical (bio) sensing applications [1–3]. For instance, gold nanoparticles (AuNPs) are responsible for improved sensitivity and stability of optical sensing properties [4–6] and imaging [7]. Thus, AuNPs represent excellent nanoplatforms in the development of various configurations of sensing chemicals and biomolecules including viruses [8,9]. In this context, the localized surface plasmon resonance (LSPR) approach is often used in (bio)sensing diagnostics by monitoring the changes in AuNPs size, shape, composition, inter-particle distance, dielectric constant (refractive index) of the surrounding medium [8,10] and the linear and/or non-linear optical properties [11]. However, before home-made AuNPs can be successfully used in clinical studies, several issues should be addressed in terms of reproducibility, reliability and stability.

In general, the most common synthesis method of AuNPs is to chemically reduce the metal salt in a solution containing a stabilizer, thereby limiting the nanoparticle's grain growth, controlling its shape and improving its stability [12]. Reducing agents, such as hydrogen, hydrazine, alcohol, carbon monoxide, Li AlH₄, NaBH₄ or R₄N⁺ (Et₃BH⁻), have been used to control the nano-size range [13]. For instance, colloidal AuNPs were synthesized by reacting chloroauric acid solution (HAuCl₄) with sodium citrate solution as the reducing and stabilizer agents [14–16]. Furthermore, on the basis of

the particle diameter and the dielectric function of AuNPs, resonance elastic light scattering (RELS) was used to monitor the ligand-exchange processes of the interactions of AuNPs with homocysteine, cysteine and glutathione biomarkers.

Although chemical reduction is convenient for synthesizing nanoparticles, it also has certain disadvantages. In addition to simplicity, this method requires extreme conditions such as high temperature and pressure, and it takes a long time to complete the reaction. The most important drawback is the nature of the reactants used in the reaction system. They are usually toxic chemicals that present potential hazard to the environment and health [17,18].

On the other hand, the aggregation of colloidal AuNPs has been used for colorimetric [19], electrochemical [20] and atomic force microscopy [21] investigations. In such applications, the choice of buffer composition is crucial for analytical performances of the sensing scheme. For example, SSPE and PBS saline buffers have been widely used for dissolving, diluting or storing active biomolecules [22–24]. In other cases, buffers were used to study the effect of electrocatalytic performances of modified electrodes for electrochemical biosensing [25–28]. However, the effect of saline buffers on the size and dispersion stability of nanoparticles on solid supports has not yet been studied.

The present paper reports on the influence of the aqueous buffers SSPE and PBS over the stability of high-annealed 4 nm gold film-coated coverslips using an optimized AuNPs synthesis protocol [29]. As it is stated in the experimental section, the annealed gold coverslips exhibit either pinkish colors when uniformity is formed or blue colors when aggregated after buffer exposure. SEM and atomic force microscope (AFM) imaging of AuNPs are collected and analyzed after dry and wet media working conditions. Furthermore, an example of BPE (1,2-bis-(4-pyridyl)-ethene) chemical sensing under optimal conditions is also discussed.

2. Materials and Methods

2.1. Chemicals

Liquid detergent Decon 90 (Decon Laboratories™ Decon 90™) was provided by Fisher Scientific (Göteborg, Sweden). Sodium chloride (NaCl, purity 99.5%), sodium phosphate monobasic and dibasic (purity 99.0%) and ethylenediaminetetraacetic acid (purity 99.0%) were provided by Sigma-Aldrich (St. Louis, MO, USA), while *trans* 1, 2-bis-(4-pyridyl)-ethene (BPE) was purchased from Sigma-Aldrich (Schnelldorf, Germany). Other chemicals were of analytical grade purity. Squared glass coverslips were provided by Carl Roth GmbH +Co. KG, (Karlsruhe, Germany).

In the preparation of saline buffers and cleaning of coverslips, ultrapure distilled water (18.2 MΩ·cm) was used, here named dd-water and produced by a Millipore Milli-Q water purification system (Molsheim, France).

2.2. Instruments

Metal evaporation was performed with Plassys MEB 400 (Bestek, France) while a hot plate (Thermo Fisher Scientific, Waltham, MA, USA) was used for thermal annealing of gold films under clean room conditions.

Nanostructured coverslips were characterized with a scanning electron microscope (SEM) (FEG-SU8030, Tokyo, Japan) and an atomic force microscope (AFM) (Bruker ICON, Billerica, MA, USA) with cantilever ScanAsyst-Air in silicon nitride with a tip height of 2.5–8.0 μm. A spring constant of 0.4 N/m and a reflective aluminum coating on the backside in standard ScanAsyst-Air mode were used to characterize the morphology of AuNPs. The AFM PeakForce mode was employed for the topographical characterization of annealed coverslips.

LSPR measurements (Figure 1) were performed with a Ø = 50 μm fiber QP50-2-UV-BX (Ocean Optics, EW Duiven, The Netherlands) coupled with an optical spectrophotometer Maya 2000 Pro and using a white exciting light source (DH-2000-BAC, Ocean Optics, EW Duiven, The Netherlands). All spectra were recorded with a 10× objective.

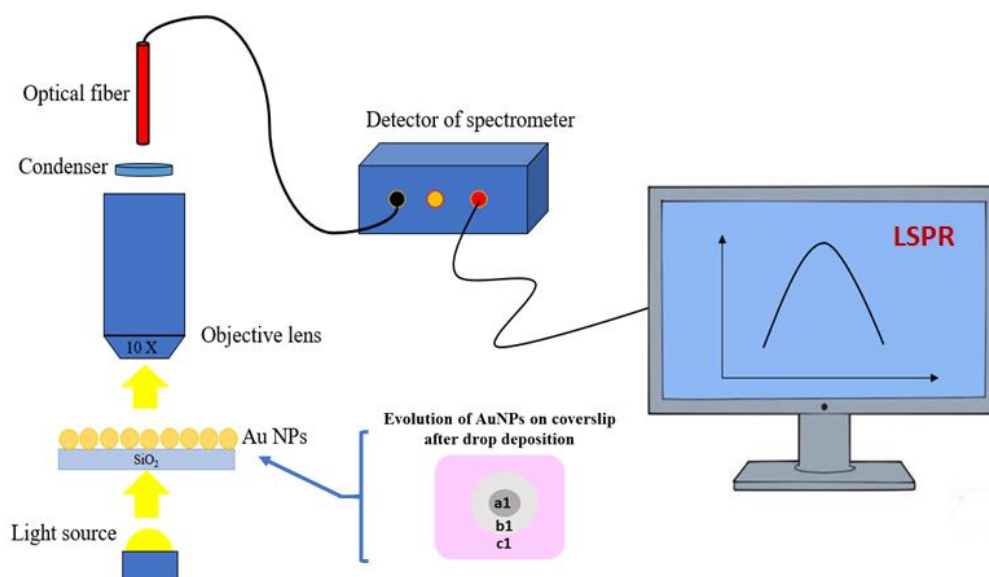


Figure 1. Set-up for localized surface plasmon resonance (LSPR) investigations of annealed gold nanoparticles (AuNPs) on coverslips exposed to drops of aqueous and saline buffers. Once the different drops of buffers were collected from the coverslips, three areas were observed and named **a1** (under the drop), **b1** (in the vicinity of the drop) and **c1** (far from the drop).

2.3. Data Analysis

SEM images were used for estimation of the size distribution of annealed nanoparticles using the Public Domain ImageJ software developed by the National Institutes of Health based on the SEM images.

Collected AFM images ($1\ \mu\text{m} \times 1\ \mu\text{m}$) were analyzed using the Gwyddion software that adjusts the colour scale according to the maximum and minimum height per line scan. This causes regions on nanostructured glass coverslips to appear darker (i.e., lower) between nanoparticles. In addition, two parameters (R_a and R_{rms}) were used to estimate the surface roughness of the annealed coverslips either in air for naked AuNPs or after exposure to water or aqueous buffers (SSPE and PBS). These parameters inform about the roughness of coverslips after different buffer treatments and count the distance between nanoparticles and valleys. Larger distances correspond to rougher surfaces.

R_a is defined as the average roughness in μm describing the overall profile height characteristics (less sensitive to large structures and valleys), while R_{rms} is the root mean square roughness of the annealed surface averaged between the height deviations and the mean line/surface taken over the evaluation length/area.

2.4. Preparation of Saline Buffers

The stock $20\times$ SSPE buffer contains 3 M sodium chloride, 0.23 M sodium phosphate dibasic and 25 mM ethylenediaminetetraacetic acid dissolved in dd-water, pH 7.4. For all experiments, $1\times$ SSPE buffer was freshly prepared.

PBS buffer contains 1.5 M sodium chloride, 81 mM sodium phosphate dibasic and 19 mM sodium phosphate monobasic dissolved in dd-water, pH 7.4. Five concentrations of BPE solutions (10^{-3} , 10^{-5} , 10^{-7} , 10^{-9} and 10^{-11} M) were prepared from 97% concentrated BPE stock using dd-water as the diluting solvent.

2.5. Preparation of Annealed Gold Nanostructures on Coverslips

There are three main steps for the fabrication of gold nanostructures on coverslips. (i) detergent cleaning: squared glass coverslips were degreased with an aqueous solution of Decon90 detergent (2:8 v/v , dd-water/detergent) in an ultrasonic distilled water bath Elmasonic S30H

(Elma Schmidbauer GmbH, Singen, Germany) at 50 °C for 15 min, followed by three times ultrasonication in a dd-water bath for 5 min at 50 °C [29]. Further, each coverslip was extensively rinsed with dd-water, dried under a nitrogen stream and placed on a hot plate at 100 °C for 10 min. (ii) gold evaporation: the cleaned substrates were fixed on a circular evaporation plate, subsequently scotch-labelled at the bottom and used for coating with gold thin (4 nm) films in an evaporator (Plassys MEB 400) using a high purity 99.99% gold source (Neyco, Vanves, France) under 1×10^{-6} Torr pressure at 25 °C with an evaporation rate of 0.01 nm/s. (iii) annealing: the 4 nm gold-coated coverslips were thermally annealed on a hot plate at 550 °C for 3 h.

2.6. Effect of Buffers over the Stability of Annealed Gold on Thin Glasses

The influence of drops of water (2 μ L), and 1 \times SSPE (2 and 5 μ L) and PBS (5 μ L) buffers on annealed gold nanostructures on coverslips was investigated using two approaches with a common step, an overnight exposure at 4 °C, in the presence of either (i) humid chamber petri dish—named “wet media”—or (ii) no petri dish—named “dry media” (Figure 2).

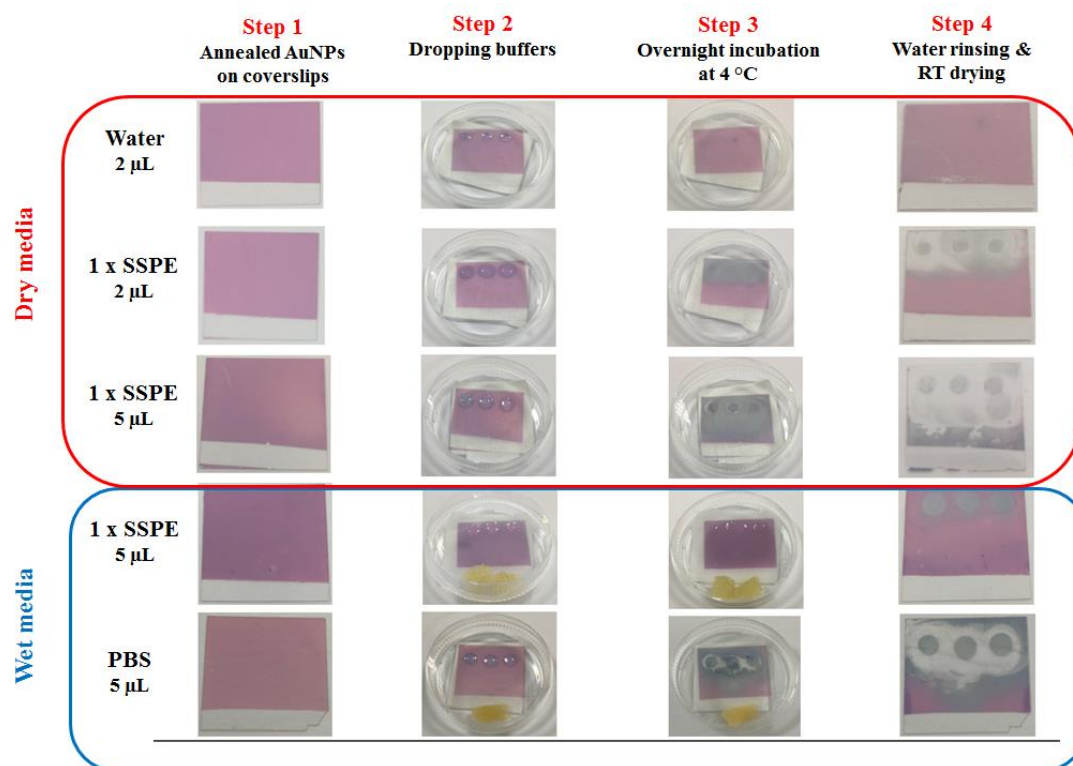


Figure 2. Naked-eye coverslips coated with annealed gold nanoparticles and exposed to wet and dry media for an overnight at 4 °C.

3. Results and Discussions

3.1. Characterization of Annealed Gold Coated Coverslips—Bare AuNPs

Microscopic (SEM, AFM) and optical (LSPR) characterizations of annealed 4 nm gold-coated coverslips were performed (Figure 3). The SEM and AFM images depict a homogeneous distribution of spherical nanoparticles that are confirmed by the size distribution in the range of 4–16 nm, where a majority of AuNPs (82%) exhibit a diameter of 8–10 nm.

The AFM image and recorded LSPR spectra also confirm the homogeneity of AuNPs from the line profile analysis with 1.410 nm R_a and 1.785 nm R_{rms} roughness values and from the overlapping of five LSPR spectra collected from five different areas of an annealed coverslip with the maximum plasmonic resonance at 542 nm.

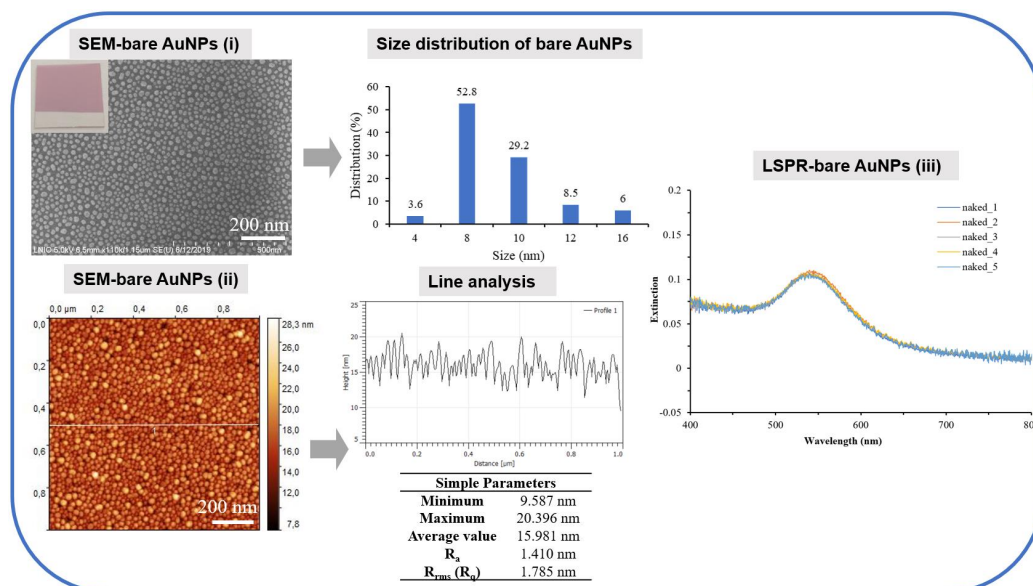


Figure 3. SEM (i), atomic force microscope (AFM) (ii) and LSPR (iii) characterizations of annealed gold nanostructured (AuNPs) coverslips. The size distribution of AuNPs (based on SEM image) and line profile analysis (based on AFM images) are also presented in the middle panel. The SEM, AFM and LSPR measurements were performed under cleanroom conditions at 21 °C.

3.2. Influence of Water and Saline Buffers over the Stability of Annealed AuNPs on Coverslips

3.2.1. Study of Water Solvent

Several surface characterization techniques were employed for the nanostructured coverslips exposed to dd-water drop (2 μ L) for several hours at 4 °C: SEM imaging with emphasized AuNPs size distribution, AFM imaging with the height profile analysis and LSPR collecting spectra (Figure 4). More specifically, on the coverslip, three areas were characterized: a1, just under the drop, b1, in the vicinity of the drop, and c1, far from the drop.

It is noticed from the SEM imaging (Figure 4i) very similar morphologies of nanoparticles whatever the tested position. Thus, the nanoparticles are spherical and homogeneously distributed. This is confirmed by the AuNPs size distribution analysis, for which no significant differences were observed. The diameter of the nanoparticles is in the majority 8–10 nm and the distribution is quite narrow. The deposition of the water drop has no significant effect on the geometry of nanoparticles and does not influence their stability on the coverslip substrate.

These observations are also confirmed by the AFM imaging (Figure 4ii) with very similar R_a (nm) (a1-2.01; b1-2.2.06; c1-2.05) and R_{ms} (nm) (a1-2.53; b1-2.57; c1-2.55) roughness values of the three selected areas. Concerning the LSPR spectra (Figure 4iii), a similar plasmonic peak evolution (λ_{max} at 559.78 nm) of the a1, b1 and c1 areas with optical density (OD) maximum values of 0.183 for NPs (a1-0.182; b1-0.182; c1-0.179) was recorded.

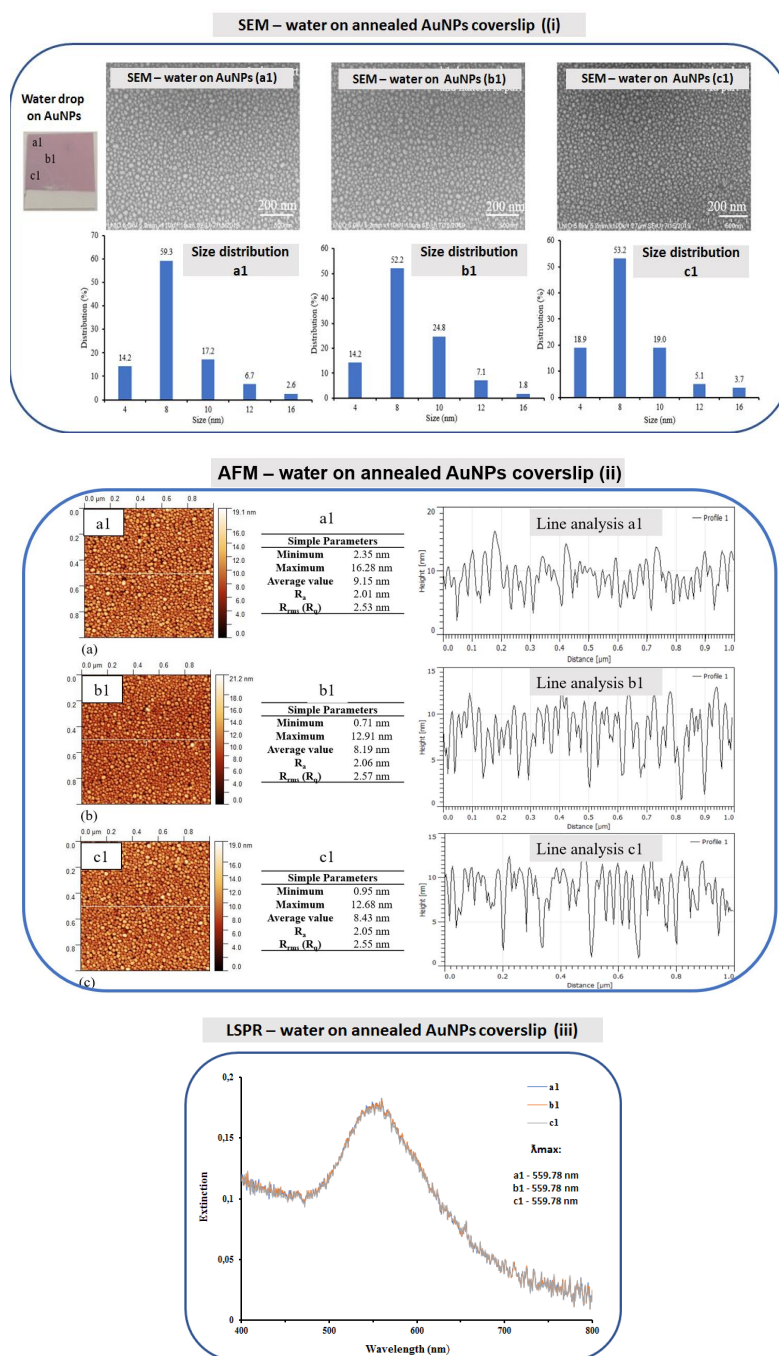


Figure 4. SEM (i), AFM (ii) and LSPR (iii) characterizations of annealed gold nanostructured (AuNPs) coverslips exposed to water drops, air dried and with three investigated areas: a1 (under the drop), b1 (in the vicinity of the drop) and c1 (far from the drop). The size distribution of AuNPs (based on SEM image) and line profile analysis (based on AFM images) were acquired for a1, b1 and c1 (dd-water, pH = 7.0). The SEM, AFM and LSPR measurements were performed under cleanroom conditions at 21 °C.

3.2.2. Study of SSPE Buffer

The SEM images in area a1 show that AuNPs form worm-like aggregates of almost ten AuNPs particles when dropped with 1× SSPE buffer under dry media (2 and 5 μ L), whereas they form smaller aggregates under wet media (5 μ L).

The SEM images in area b1 show a similar morphology under dry media than this one observed under wet media in area a1. AuNPs are almost absent on the substrate for the highest buffer concentration under the dry condition. Under the wet condition, the aspect of the AuNPs is very similar to this one observed for the annealed AuNPs in Figure 2.

The SEM images (Figure 5i) in area c1 show a similar morphology for 1× SSPE buffer under dry media (A) and for the wet media (C) than was also observed for the annealed AuNPs in Figure 2. For the 5 μ L buffer under dry media (B), the images evidence some aggregates.

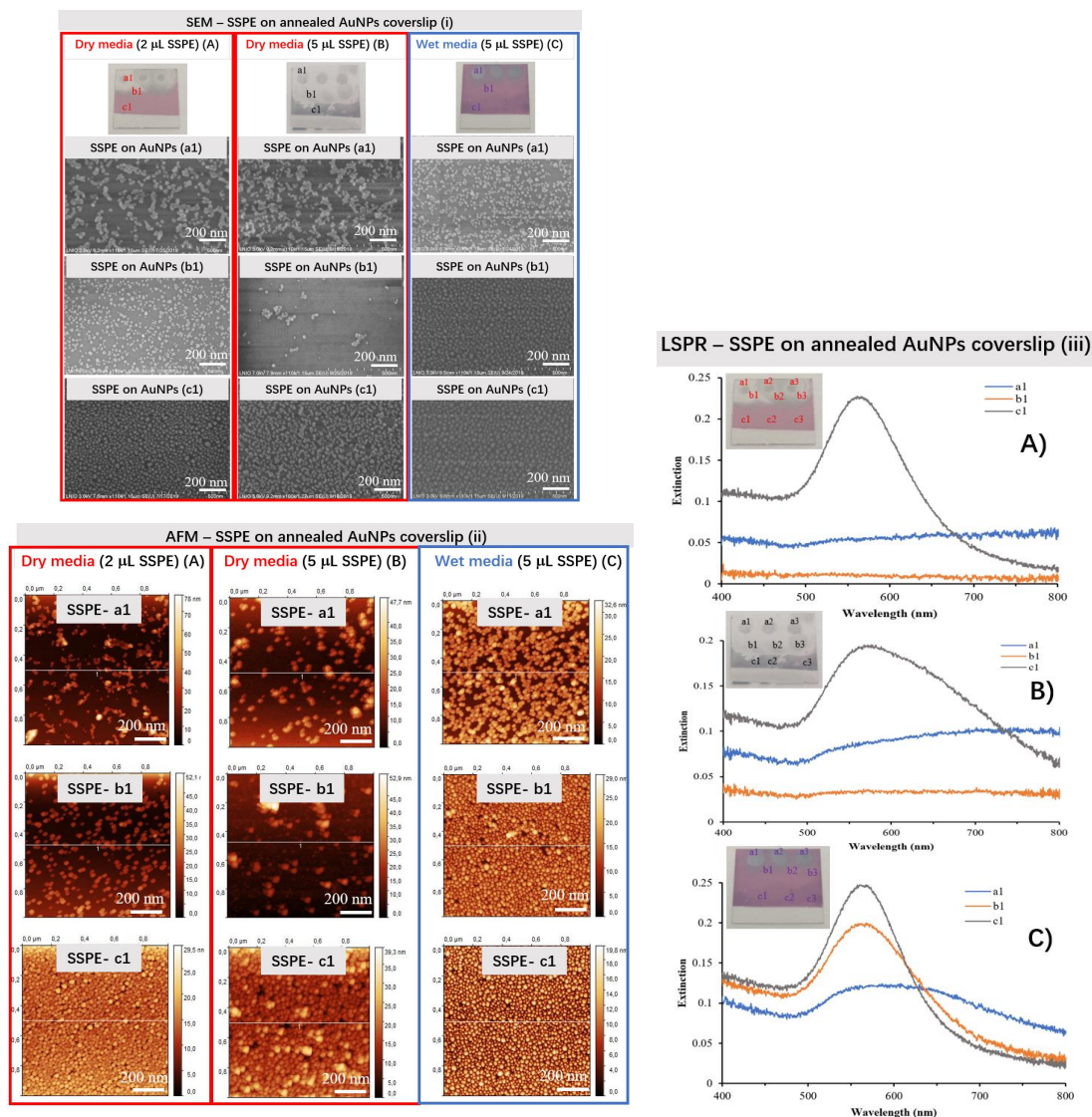


Figure 5. SEM (i), AFM (ii) and LSPR (iii) characterizations of annealed gold nanostructured (AuNPs) coverslips exposed to three drops of SSPE per coverslip with three areas investigated for each deposited/removed drop (a1, under the drop, b1, in the vicinity of the drop, and c1, far from the drop). Two approaches were tested (A) 2 μ L SSPE drop and (B) 5 μ L SSPE drop on coverslip for an overnight at 4 $^{\circ}$ C under dry media; (C) 5 μ L SSPE drop on coverslip for an overnight at 4 $^{\circ}$ C under wet media (1 \times SSPE buffer, pH = 7.4). The SEM, AFM and LSPR measurements were performed under cleanroom conditions at 21 $^{\circ}$ C.

To conclude, the dropping of 1 \times SSPE buffer clearly affects the morphology and the stability of annealed AuNPs on coverslips, especially under dry media and strongly in the presence of 5 μ L buffer under wet conditions.

The size distribution of AuNPs (based on SEM image) and line profile analysis (based on AFM images) (Figure 5ii) were also acquired for the a1, b1 and c1 areas. Moreover, the variation in the R_{rms} values (data not shown), that are similar for the dry (b1—4.977 nm) and wet media (b1—3.852 nm), showed no further changes on area c1 but strongly affected area a1 for both conditions. The highest R_{rms} value is observed for the buffer content of 2 μ L 1 \times SSPE in dry condition in area a1—7.638 nm, probably due to the faster evaporation of the drop.

As expected, similar LSPR resonant spectra with a maximum of extinction versus wavelength were obtained for the naked AuNPs presented on the c1 area of samples under dry and wet media. For the b1 area under dry media, no plasmonic peak spectra are recorded contrary to a well-defined spectrum for the sample under wet media. Concerning the a1 zone for all tested samples, no LSPR peak was possible (Figure 5iii).

In conclusion, the protocol of annealed AuNPs under wet media shows good particle stability on coverslips and it was used for PBS buffer study.

3.2.3. Study of PBS Buffer

Three drops of 5 μ L PBS buffer were placed on annealed AuNPs and kept under wet media for overnight at 4 $^{\circ}$ C. The SEM images (Figure 6i) depict a similar behavior of agglomeration of nanoparticles in chains (a1 area) close to those images obtained in the presence of SSPE buffer (5 μ L), but under dry media. Very few AuNPs are observed in the b1 area, suggesting a stronger destabilization effect of the PBS buffer over the annealed NPs. These observations are also confirmed by AFM imaging (Figure 6ii) and the corresponding line profile analysis with R_{rms} roughness values of 6.33 for a1, 1.94 for b1 and 2.91 nm for c1.

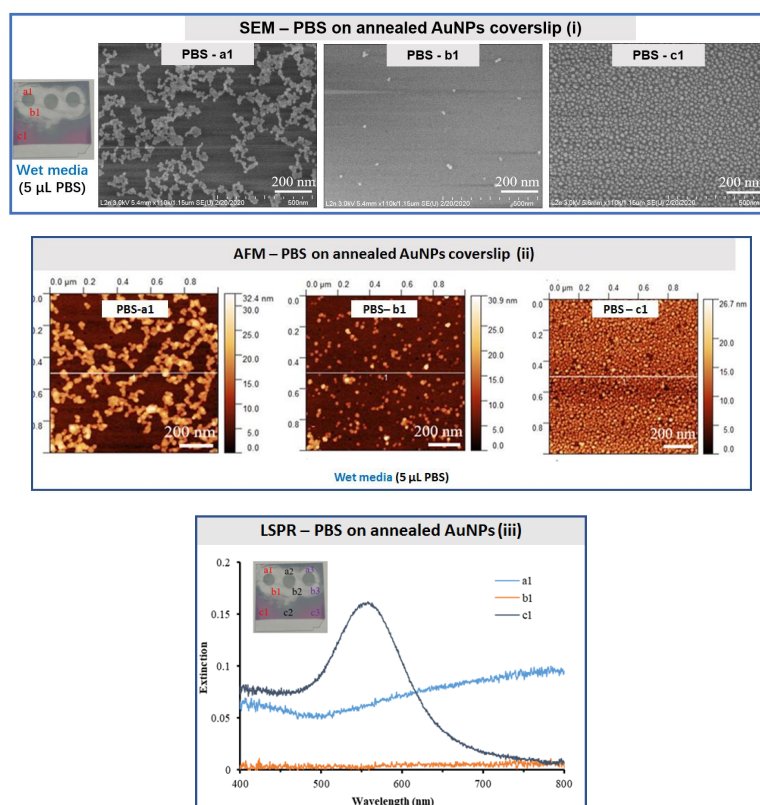


Figure 6. SEM (i), AFM (ii) and LSPR (iii) characterizations of annealed gold nanostructured (AuNPs) coverslips exposed to three drops of PBS (5 μ L) per coverslip under wet media with three areas investigated for each deposited/removed drop: a1, under the drop, b1, in the vicinity of the drop, and c1, far from the drop (10 \times PBS buffer, pH = 7.4). The SEM, AFM and LSPR measurements were performed under cleanroom conditions at 21 $^{\circ}$ C.

The LSPR spectra were collected from annealed AuNPs after the deposition of three PBS drops with three tested areas (a1, b1 and c1) per drop. A resonant plasmonic peak was recorded from area c1, while no peaks were noted for areas a1 and b1 (Figure 6iii).

3.3. Sensing of Chemical BPE Molecules in Aqueous Solution with SEM, AFM and LSPR Characterization

Based on the previous results on the stability of annealed AuNPs on coverslips in the presence of a water solvent, the functionalization of AuNPs in the presence of model BPE molecules in aqueous solution was investigated.

The SEM images (data not shown) show dense, homogeneous and spherical AuNPs after treatment with BPE solutions. The NPs size distribution is distributed in a narrow range from 4 to 16 nm. For instance, the 8 nm AuNPs are the mostly formed particles on the coverslips (52.8%) and further modified by exposure to five BPE concentrations: 10^{-3} M (30.3%), 10^{-5} M (49.8%), 10^{-7} M (48.3%), 10^{-9} M (50.6%) and 10^{-11} M (46.6%). Other NPs sizes varied from $10 > 12 > 16$ nm for both exposed and not exposed to BPE concentrations. No significant size differences between the naked and BPE-exposed AuNPs are observed. However, as the BPE concentration increased, the presence of gaps between the nanoparticles was observed.

The AFM imaging of the BPE-modified AuNPs (Figure 7) confirms the homogeneous surface morphology of AuNPs on the coverslips shown with SEM images, with no large R_{rms} differences (3.53 to 4.55 nm) for the five BPE concentrations but higher than the naked AuNPs ($R_{rms} = 2.55$).

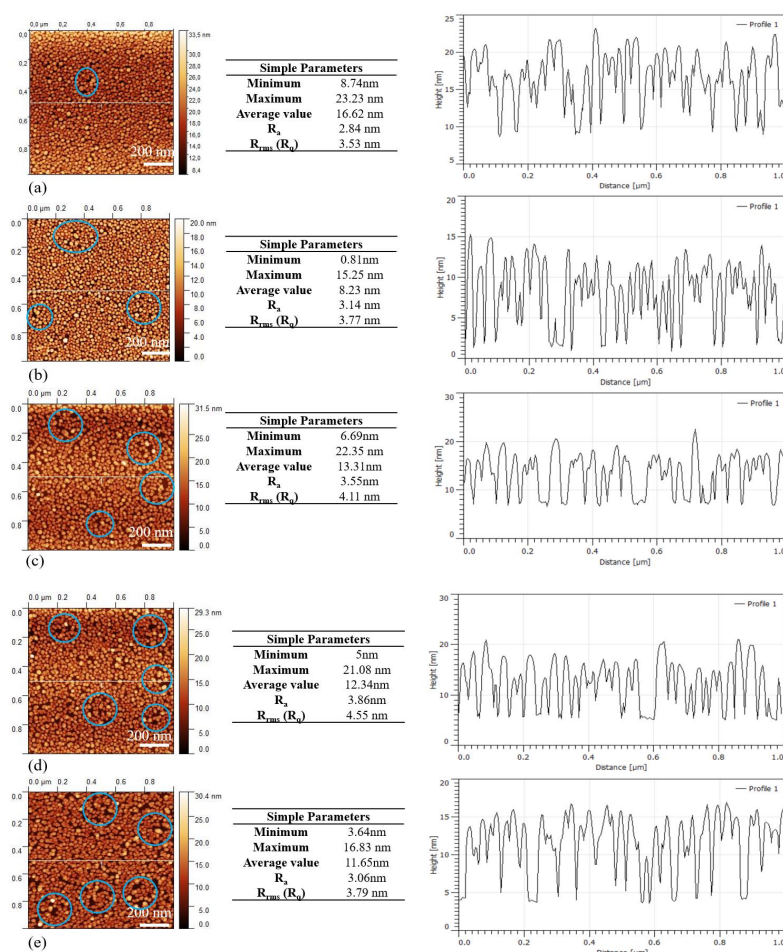


Figure 7. AFM images of annealed AuNPs modified by different concentrations of BPE model molecules, cross-section analysis was based on the profile line analysis. (a) 10^{-3} M BPE; (b) 10^{-5} M BPE; (c) 10^{-7} M BPE; (d) 10^{-9} M BPE; (e) 10^{-11} M BPE. The AFM measurements were performed under cleanroom conditions at 21 °C.

The evolution of LSPR spectra of annealed AuNPs exposed to BPE concentrations over five weeks was investigated (Figure 8). Moreover, the values of the maximum resonant wavelength length with its corresponding maximum optical density (OD_{max}) are reported in Table 1. Additionally, reproducible LSPR spectra were collected from larger coverslip areas (about 1 cm²).

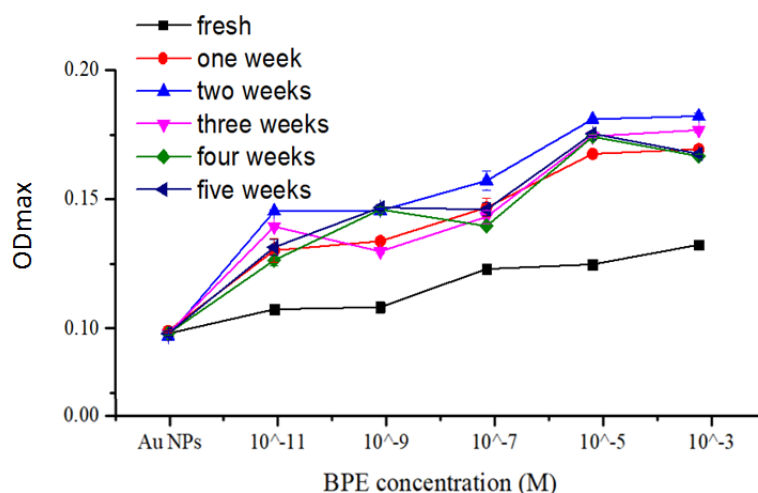


Figure 8. Evolution of maximum optical density (OD_{max}) of annealed AuNPs functionalized with five BPE concentrations over five weeks (fresh—the day of functionalization). The coverslip was evaporated with 4 nm Au and annealed at 550 °C for 3 h.

Table 1. Evolution of LSPR spectra of AuNPs functionalized with different BPE concentrations over five weeks. The LSPR measurements were performed under cleanroom conditions at 21 °C.

[BPE]		Fresh Functionalization	After One Week	After Two Weeks	After Three Weeks	After Four Weeks	After Five Weeks
10 ⁻³ M	λ_{max} (nm)	548.210	549.904	550.792	553.910	552.660	552.660
	OD_{max}	0.13240	0.16940	0.18220	0.17680	0.16668	0.16760
10 ⁻⁵ M	λ_{max} (nm)	548.566	549.814	550.260	553.110	552.660	552.660
	OD_{max}	0.12480	0.16760	0.18100	0.17440	0.17420	0.17540
10 ⁻⁷ M	λ_{max} (nm)	550.706	549.636	548.566	553.110	559.780	552.660
	OD_{max}	0.12300	0.14680	0.15720	0.14320	0.13960	0.14600
10 ⁻⁹ M	λ_{max} (nm)	551.864	551.062	550.440	553.288	559.780	559.780
	OD_{max}	0.10820	0.13380	0.14560	0.12980	0.14600	0.14680
10 ⁻¹¹ M	λ_{max} (nm)	551.864	539.290	542.412	548.654	559.870	552.660
	OD_{max}	0.10740	0.13020	0.14540	0.13940	0.12640	0.13140

The lower tested concentration 10⁻¹¹ M of BPE is detectable using annealed AuNPs on coverslips. The OD_{max} values increased from the day of nanoparticle functionalization with five BPE concentrations up to 14 days. After two weeks, the OD_{max} values were decreasing but were still higher than those obtained in the day of functionalization (named Fresh). It is noticed that λ_{max} values increased as expected from 10⁻¹¹ to 10⁻³ M BPE with the coated annealed AuNPs from the preparation day to the third week. After the third and fourth weeks, the plasmonic properties are strongly degraded.

To conclude, by comparing both plasmonic parameters (λ_{max} , OD_{max}), two weeks testing is recommended for an LSPR investigation of the stability of BPE functionalized AuNPs on coverslips.

4. Conclusions

In this work, high-annealed AuNPs were prepared on thin coverslips at a large scale, showing homogeneity and well-defined plasmonic resonant peaks. Knowing the important roles of biological

buffers (for instance SSPE and PBS) in the aliquots and (bio) functionalization preparation steps, SEM/AFM/LSPR studies of nanoparticles stability in the presence of these buffers are herein reported. The influence of tiny drops of dd-water and BPE aqueous solutions for sensing on an annealed gold nanoparticles surface is also investigated. Dry and wet media working configurations were tested by dropping buffers on AuNPs. No effect in the presence of dd-water was remarked, while SSPE and PBS destabilized the annealed AuNPs under dry media. However, the AuNPs are less affected by saline SSPE and PBS buffers under 4 °C wet media. LSPR sensing of 10^{-11} M BPE was also possible on AuNPs with good plasmonic signal stability over two weeks.

Author Contributions: Conceptualization, R.E.I.; formal analysis, L.Z.; funding acquisition, R.E.I.; investigation, L.Z.; methodology, R.E.I.; software, L.Z.; supervision, R.E.I.; writing—original draft, L.Z.; writing—review and editing, R.E.I. All authors have read and agreed to the published version of the manuscript.

Funding: This research was funded by Agence Nationale de la Recherche, grant number ANR-20-COVI-0080.

Acknowledgments: The authors thank ANR Flash Covid-19 for funding AcOstoVie project and the Nanomat Champagne-Ardenne Regional Platform. L. Zhou kindly thanks the Chinese Scholarship Council (CSC) for funding her PhD scholarship in France (October 2017–April 2021).

Conflicts of Interest: The authors declare no conflict of interest.

References

1. Malekzad, H.; Zangabad, P.S.; Mirshekari, H.; Karimi, M.; Hamblin, M.R. Noble metal nanoparticles in biosensors: Recent studies and applications. *Nanotechnol. Rev.* **2017**, *6*, 301–329. [[CrossRef](#)]
2. Cogley, C.M.; Chen, J.; Cho, E.C.; Wang, L.V.; Xia, Y. Gold nanostructures: A class of multifunctional materials for biomedical applications. *Chem. Soc. Rev.* **2011**, *40*, 44–56. [[CrossRef](#)]
3. You, Z.; Qiu, Q.; Chen, H.; Feng, Y.; Wang, X.; Wang, Y.; Ying, Y. Laser-induced noble metal nanoparticle-graphene composites enabled flexible biosensor for pathogen detection. *Biosens. Bioelectron.* **2020**, *150*, 111896. [[CrossRef](#)] [[PubMed](#)]
4. Presnova, G.; Presnov, D.; Krupenin, V.; Grigorenko, V.; Trifonov, A.; Andreeva, I.; Ignatenko, O.; Egorov, A.; Rubtsova, M. Biosensor based on a silicon nanowire field-effect transistor functionalized by gold nanoparticles for the highly sensitive determination of prostate specific antigen. *Biosens. Bioelectron.* **2017**, *88*, 283–289. [[CrossRef](#)]
5. Qin, L.; Zeng, G.; Lai, C.; Huang, D.; Xu, P.; Zhang, C.; Cheng, M.; Liu, X.; Liu, S.; Li, B.; et al. “Gold rush” in modern science: Fabrication strategies and typical advanced applications of gold nanoparticles in sensing. *Coord. Chem. Rev.* **2018**, *359*, 1–31. [[CrossRef](#)]
6. Qu, F.; Huang, W.; You, J. A fluorescent sensor for detecting dopamine and tyrosinase activity by dual-emission carbon dots and gold nanoparticles. *Colloids Surf. B Biointerfaces* **2018**, *162*, 212–219. [[CrossRef](#)] [[PubMed](#)]
7. Wu, Y.; Ali, M.R.K.; Chen, K.; Fang, N.; El-Sayed, M.A. Gold nanoparticles in biological optical imaging. *NanoToday* **2019**, *24*, 120–140. [[CrossRef](#)]
8. Zeng, S.; Yong, K.-T.; Roy, I.; Dinh, X.-Q.; Yu, X.; Luan, F. A Review on functionalized gold nanoparticles for biosensing applications. *Plasmonics* **2011**, *6*, 491–506. [[CrossRef](#)]
9. Guliy, O.I.; Kanevskiy, M.V.; Fomin, A.S.; Staroverov, S.A.; Bunin, V.D. Progress in the use of an electro-optical sensor for virus detection. *Opt. Commun.* **2020**, *465*, 125605. [[CrossRef](#)]
10. Alharbi, R.; Irannejad, M.; Yavuz, M. A short review on the role of the metal-graphene hybrid nanostructure in promoting the localized surface plasmon resonance sensor performance. *Sensors* **2019**, *19*, 862. [[CrossRef](#)]
11. Jatschka, J.; Dathe, A.; Csáki, A.; Fritzsche, W.; Stranik, Q. Propagating and localized surface plasmon resonance sensing—A critical comparison based on measurements and theory. *Sens. Bio Sens. Res.* **2016**, *7*, 62–70. [[CrossRef](#)]
12. Daniel, M.C.; Astruc, D. Gold nanoparticles: assembly, supramolecular chemistry, quantum-size-related properties, and applications toward biology, catalysis, and nanotechnology. *Chem. Rev.* **2004**, *104*, 293–346. [[CrossRef](#)] [[PubMed](#)]
13. Schmid, G.; Chi, L.F. Metal clusters and colloids. *Adv. Mater.* **1998**, *10*, 515–526. [[CrossRef](#)]
14. Stobiecka, M.; Deeb, J.; Hepel, M. Ligand exchange effects in gold nanoparticle assembly induced by oxidative stress biomarkers: Homocysteine and cysteine. *Biophys. Chem.* **2010**, *146*, 98–107. [[CrossRef](#)]

15. Stobiecka, M.; Coopersmith, K.; Hepel, M. Resonance elastic light scattering (RELS) spectroscopy of fast non-Langmuirian ligand-exchange in glutathione-induced gold nanoparticle assembly. *J. Colloid Interface Sci.* **2020**, *350*, 168–177. [[CrossRef](#)]
16. Stobiecka, M.; Hepel, M. Rapid functionalization of metal nanoparticles by moderator-tunable ligand-exchange process for biosensor designs. *Sens. Actuators B Chem.* **2020**, *149*, 373–380. [[CrossRef](#)]
17. Jain, N.; Bhargava, A.; Majumdar, S.; Tarafdar, J.C.; Panwar, J. Extracellular biosynthesis and characterization of silver nanoparticles using *Aspergillus flavus* NJP08: A mechanism perspective. *Nanoscale* **2011**, *3*, 635–641. [[CrossRef](#)]
18. Narayanan, K.B.; Sakthivel, N. Mycocrystallization of gold ions by the fungus *Cylindrocladium floridanum*. *World J. Microbiol. Biotechnol.* **2013**, *29*, 2207–2211. [[CrossRef](#)]
19. Singh, R.; Thakur, P.; Thakur, A.; Kumar, H.; Chawla, P.; V. Rohit, J.; Kaushik, R.; Kumar, N. Colorimetric sensing approaches of surface-modified gold and silver nanoparticles for detection of residual pesticides: A review. *Int. J. Environ. Anal. Chem.* **2020**, 1–17, in press. [[CrossRef](#)]
20. Chiorcea-Paquim, A.-M.; Eritja, R.; Oliveira-Brett, A.M. Electrochemical and AFM characterization of G-quadruplex electrochemical biosensors and applications. *J. Nucleic Acids* **2018**, *2018*, 5307106. [[CrossRef](#)]
21. Li, Q.; Zhang, T.; Pan, Y.; Ciacchi, L.C.; Xu, B.; Wei, G. AFM-based force spectroscopy for bioimaging and biosensing. *RSC Adv.* **2016**, *6*, 12893–12912. [[CrossRef](#)]
22. Manzano, M.; Vizzini, P.; Jia, K.; Adam, P.-M.; Ionescu, R.E. Development of localized surface plasmon resonance biosensors for the detection of *Brettanomyces bruxellensis* in wine. *Sens. Actuators B Chem.* **2016**, *223*, 295–300. [[CrossRef](#)]
23. Miranda-Castro, R.; Sánchez-Salcedo, R.; Suárez-Álvarez, B.; Los-Santos-Álvarez, N.; Miranda-Ordieres, A.J.; Lobo-Castañón, M.J. Thioaromatic DNA monolayers for target-amplification-free electrochemical sensing of environmental pathogenic bacteria. *Biosens. Bioelectron.* **2017**, *92*, 162–170. [[CrossRef](#)] [[PubMed](#)]
24. Batule, B.S.; Seok, Y.; Kim, M.-G. Paper-based nucleic acid testing system for simple and early diagnosis of mosquito-borne RNA viruses from human serum. *Biosens. Bioelectron.* **2020**, *151*, 111998. [[CrossRef](#)]
25. Liu, L.; Wei, Y.; Jiao, S.; Zhu, S.; Liu, X. A novel label-free strategy for the ultrasensitive miRNA-182 detection based on MoS₂/Ti₃C₂ nanohybrids. *Biosens. Bioelectron.* **2019**, *137*, 45–51. [[CrossRef](#)]
26. Hamid, R.; Zhad, L.Z.; Rodríguez Torres, Y.M.; Lai, R.Y. A reagentless and reusable electrochemical aptamer-based sensor for rapid detection of Cd (II). *J. Electroanal. Chem.* **2017**, *803*, 89–94.
27. Tan, Y.; Qiu, J.; Cui, M.; Wei, X.; Zhao, M.; Qiu, B.; Chen, G. An immobilization free DNAzyme based electrochemical biosensor for lead determination. *Analyst* **2016**, *141*, 1121–1126. [[CrossRef](#)]
28. Akhtar, N.; Emran, M.Y.; Shenashen, M.A.; Khalifa, H.; Osaka, T.; Faheem, A.; Homma, T.; Kawarada, H.; El-Safty, S.A. Fabrication of photo-electrochemical biosensors for ultrasensitive screening of mono-bioactive molecules: The effect of geometrical structures and crystal surfaces. *J. Mater. Chem. B* **2017**, *5*, 7985–7996. [[CrossRef](#)]
29. Zhou, L.; Poggesi, S.; Casari Bariani, G.; Mittapalli, R.; Adam, P.-M.; Manzano, M.; Ionescu, R.E. Robust SERS platforms based on annealed gold nanostructures formed on ultrafine glass substrates for various (bio)applications. *Biosensors* **2019**, *9*, 53. [[CrossRef](#)]

